Calcium Involvement in Regulation of Neuronal Bursting in Disinhibited Neuronal Networks: Insights from Calcium Studies in a Spherical Cell Model

Pawel Kudela,* Gregory K. Bergey, and Piotr J. Franaszczuk
Department of Neurology, The Johns Hopkins Epilepsy Center, The Johns Hopkins University School of Medicine, Baltimore, Maryland

ABSTRACT Cytosolic calcium is involved in the regulation of many intracellular processes. Intracellular calcium may therefore potentially affect the behavior of both single neurons and synaptically connected neuronal assemblies. In computer model studies, we investigated calcium dynamics in spherical neurons during periods of recurrent neuronal bursting that were simulated in a disinhibited neuronal network. The model takes into account calcium influx via voltage-gated calcium channels, extrusion through the cell membrane, and binding to two different buffers representing fixed and mobile endogenous calcium buffers. Throughout the duration of the simulated recurrent neuronal bursting, the concentration of free fixed buffers shows a hyperbolic decrease in time at a rate that is not uniform inside a neuron. Recurrent calcium influxes associated with bursting lead to the formation of gradients in the concentration of the fixed buffer in the radial direction, and are accompanied by the redistribution of mobile buffers acting to compensate for these gradients. Simulated intracellular calcium transients have a slow component characterized by a gradual increase in the calcium baseline level that reaches a plateau 120–200 s after the onset of recurrent bursting. Using this model, we demonstrate what we believe is a novel mechanism of regulation of network excitability that occurs in conditions of prolonged and recurrent neuronal bursting in disinhibited networks. This mechanism is expressed via interaction of calcium clearance systems inside neurons with calcium-dependent potassium regulation of neuronal excitability in membranes. This is a network phenomenon because it arises largely by synaptic interactions. Therefore, it can serve as a network safety mechanism to prevent excessive and uncontrolled neuronal firing resulting from the lack of inhibition or after acute suppression of the inhibitory drive.

INTRODUCTION

Calcium ions (Ca^{2+}) have received special attention because of their widespread role in cellular signaling and their involvement in a variety of cell regulatory mechanisms. Ca^{2+} ions play a ubiquitous role in a number of essential cellular events, including the release of transmitters in synaptic terminals, intracellular Ca^{2+} release, control of membrane excitability, and activation of enzymes and genes. Ca^{2+} is also thought to play an essential role in synaptic plasticity and learning. Among the many regulatory functions that Ca^{2+} provides in cells, one of the most important is the activation of Ca^{2+}-dependent K channels (K_{Ca}), which carry the $I_{K(Ca)}$ current (1). The slow afterhyperpolarization (sAHP) that follows a burst or train of action potentials (APs) and results from activation of the $I_{K(Ca),sAHP}$ (sAHP current) represents an important negative feedback that controls neuronal excitability. The I_{sAHP} current is prominent in many excitatory neurons that exhibit spike frequency adaptation. Spike firing adaptation, in contrast to synaptic plasticity, represents a nonsynaptic form of neuronal plasticity. Regardless of the type of plasticity, an increased cytosolic calcium concentration ($[Ca^{2+}]_i$) seems to be a common denominator because it precedes changes in synaptic efficacy and membrane excitability. Both synaptic plasticity and firing adaptation can change the behavior of synaptically connected neurons and affect the evolution of the network activity pattern. Yet despite its importance, evidence linking $[Ca^{2+}]_i$ and neuronal membrane excitability with network dynamics and evolution of network patterns is limited.

Intracellular Ca^{2+} diffusion, binding, and uptake can be studied theoretically in cell computer models. To investigate how $[Ca^{2+}]_i$ affects the evolution of a neuronal network pattern in a longer time window, a detailed $[Ca^{2+}]_i$ dynamics model must be considered. Exact information about intracellular Ca^{2+} spread and distribution in a cell is necessary to understand the many important functions of Ca^{2+} as an intracellular messenger.

In this study, we show how excitatory neurons that are synaptically connected in a neuronal network may use intracellular Ca^{2+} not only to regulate their membrane excitability, but also to control the network bursting pattern. We addressed these issues by performing computational studies of the Ca^{2+} dynamics in a spherical cell model throughout the duration of epileptiform-like activity that was simulated in disinhibited neuronal networks. Using this theoretical model of $[Ca^{2+}]_i$ spread and distribution in cells, we demonstrate that throughout the duration of the simulated epileptiform activity, $[Ca^{2+}]_i$ dynamics has a very slow component. It is characterized by a gradual increase in the $[Ca^{2+}]_i$ baseline level in neurons, typically reaching a plateau 120–180 s after the onset of a recurrent bursting in the network. These analyses helped us to identify what we believe is a novel mechanism of regulation of neuronal bursting activity that occurs in conditions of prolonged and recurrent neuronal bursting. We demonstrate

Submitted February 12, 2009, and accepted for publication September 14, 2009.

*Correspondence: pkudela@jhmi.edu

Editor: Arthur Sherman.

0006-3495/09/12/3065/10 $2.00

doi: 10.1016/j.bpj.2009.09.027

that this mechanism is expressed via interaction of $[Ca^{2+}]_i$ clearance systems inside cells with Ca^{2+}-dependent K^+ regulation of membrane excitability in cell membranes. We conclude that this mechanism arises largely throughout synaptic interactions of neurons in a network. We suggest that in cortical or hippocampal neuronal assemblies, it may serve as a network safety mechanism to prevent excessive and uncontrolled neuronal firing resulting from the lack of inhibition or after the acute suppression of inhibitory neurons.

METHODS

Model of active membrane

Neurons are simulated as single compartments by using a conductance-based model. The model of active membrane includes sodium, calcium, potassium, as well as Na^+/Ca^{2+} exchange current (I_{NaCa}). Sodium and potassium are Hodgkin-Huxley type currents, and the calcium currents are modeled with the Goldman-Hodgkin-Katz equation. The I_{NaCa} current exhibits both voltage and ion transmembrane electrochemical gradient dependence. Two types of neurons are simulated: 1), excitatory cells, which are regular spiking neurons that exhibit spike frequency adaptation; and 2), inhibitory interneurons, which are modeled as fast-spiking neurons. The firing adaptation in the model results from the spike AHP and is produced by the slow voltage-insensitive $I_{K(Ca),sAHP}$ current. The equations and parameters of the active currents in the membrane model are provided in the Supporting Material and can also be found elsewhere (2,3).

Model of a network

A neuronal network model consists of an array of $n \times n$ excitatory and $m \times m$ inhibitory interneurons uniformly distributed in a two-dimensional plane with either open or periodic boundary conditions. The size of the network varies from 1440 ($n = 36$; $m = 12$) to 61,200 ($n = 240$; $m = 60$) neurons (the fraction of interneurons varies from 6% to 10%, respectively). To make the population of neurons heterogeneous, the parameters of the membrane model are lognormally distributed in neurons across the network with a given mean value and a 15% standard deviation. Inhibitory neurons make synaptic contacts locally with neighboring excitatory and inhibitory interneurons. Excitatory neurons form synapses with neighboring inhibitory interneurons and can make long-range connections with remote excitatory neurons. The probability of long-range connections decreases exponentially with distance, whereas synaptic delays increase linearly with distance. Synaptic contacts have synaptic weights and delays assigned with a given mean value and a 15% standard deviation. In these networks, each neuron has a minimum of two excitatory synapses on input from randomly selected presynaptic neurons. The strength of the excitatory synapses is adjusted to the level that allows the spread of bursting activity from pre- to postsynaptic excitatory neurons throughout the network when the interneurons are not active. The induction of bursts in excitatory neurons includes acute or gradual suppression of the excitatory drive to interneurons. In a typical simulation, interneurons in the network are suppressed a few seconds after the beginning of a simulation and remain silent throughout the rest of the simulation.

Model of calcium dynamics

The model of Ca^{2+} dynamics includes entry of Ca^{2+} into the cell via different Ca^{2+}-permeable channels, Ca^{2+} binding to buffers, Ca^{2+} diffusion throughout the cell body, and efflux via the Ca pumps. Two types of endogenous Ca^{2+} buffer systems—B and Bs—are simulated. Type B aims to represent intrinsic protein (calmodulin, calbindin, and calcineurin), which are mobile, kinetically fast-acting buffers with relatively low capacity. Type Bs is defined as kinetically slow fixed buffers with high capacity and is designated to simulate endoplasmic reticulum uptake. In the simulations, the parameters for both the mobile and fixed buffer systems vary in a range representative of mammalian hippocampal cells. The total buffer concentrations $[B]_i^{total}$ vary from 50 to 200 μM, whereas $[Bs]_i^{total}$ are in the range of 600–1800 μM. A spherical model of a cell body with a radius of 20 μm is used in simulations. Simplified cell representation results from a compromise between the ability to undertake Ca^{2+} modeling and the cell morphology. Ca^{2+} diffusion inside a cell is simulated in a radial direction by using the finite-difference approximation formula for a sphere. This requires discretization of a sphere into a series of equally spaced concentric shells. Ca^{2+} influx via Ca^{2+} channels and extrusion via Ca pumps are simulated in the outermost shell. The rate of Ca^{2+} entry into a cell depends on the amplitude of the calcium currents (L-, N-, and T-type). The kinetics and rate constants for these currents are based on data from hippocampal neurons. The process of Ca^{2+} extrusion by the Na^+/Ca^{2+} exchanger is modeled in the outermost shell. The plasmalemmal calcium ATPase (PMCA) pump is modeled in the outermost shell as a process that obeys first-order Michaelis-Menten kinetics (see the Supporting Material for all details).

RESULTS

Acute suppression of inhibitory interneurons in a simulated network leads to epileptiform-like activity, which manifests in excitatory neurons as a synchronous and recurrent burst firing. Fig. 1 shows the number of APs fired by excitatory neurons as a function of time. Fig. 1 *a* illustrates the initial 10 s of a typical simulation. When interneurons are active (0–4 s), the number of APs fired by excitatory neurons varies slightly, with an average of 200 (1440 neurons, 10 ms bin). Shortly (i.e., 4–6 s) after the withdrawal of excitatory input to interneurons that occurs at $t = 4$ s, the number of APs oscillates between 0 and 1000 ($t > 8$ s). The emergence of the oscillation in the number of APs fired by excitatory neurons indicates the onset of epileptiform activity in the network. The frequency at which excitatory neurons are activated and fire trains of APs varies throughout the duration of the simulated epileptiform activity, with the highest frequencies occurring after the suppression of inhibitory neurons. Fig. 1, *b* and *c*, show the numbers of APs fired by excitatory neurons, in 1-s-long periods, at the 12th and 69th s of the simulation. These numbers oscillate at 7.5 and 3 Hz, respectively, which corresponds to the occurrence of bursts in neurons with burst-to-burst intervals equal to ~135 ms (panel *b*) and 330 ms (panel *c*), respectively.

Typically, the frequency of burst occurrence (bursts/s) in a network decreases from 6–8 Hz to ~1–4 Hz, at a rate of 2–4 Hz/min, depending on the values of the parameters used in a simulation. Fig. 1 *d* shows an example of a pattern of a burst frequency decline in a 300-s-long simulation as measured in a population of excitatory neurons. The points represent instant frequencies and were obtained by taking the inverse of burst-to-burst intervals. The onset of the bursting activity was positioned at $t = 0$. The period after the onset is dominated by burst frequencies in the range 5–8 Hz. Later, these frequencies decrease throughout the duration of the simulated epileptiform activity to ~2 Hz. For a comparison, the top-right inset (control) shows a pattern of AP frequencies obtained in a simulation when inhibition was present. In the

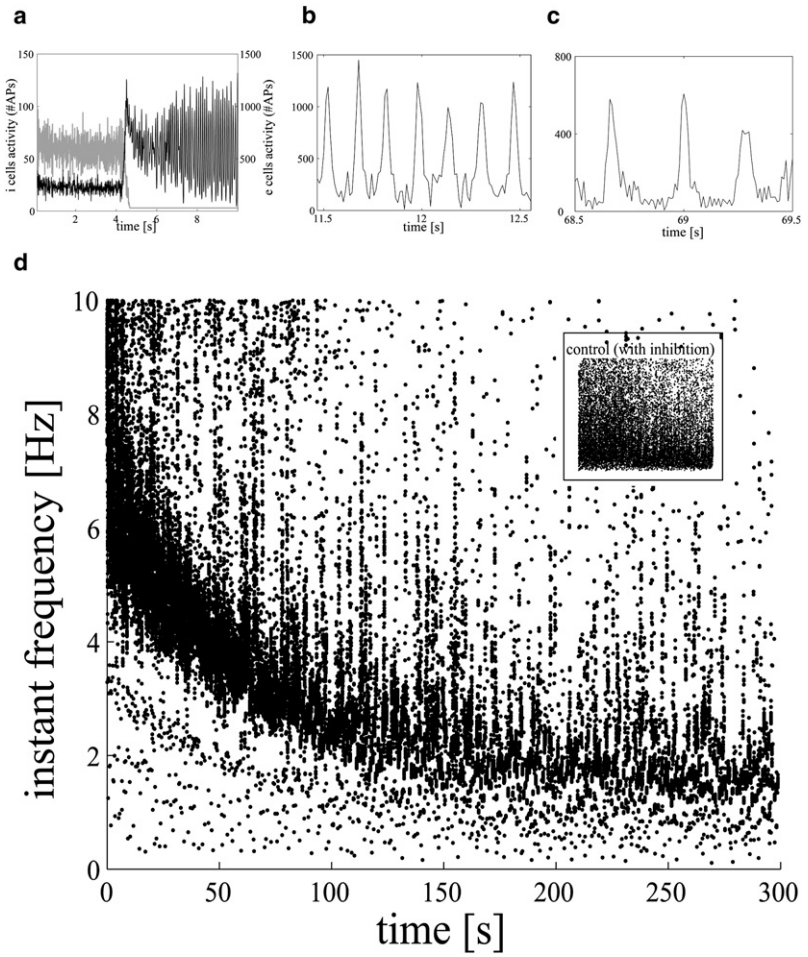

FIGURE 1 (*a*) Number of APs fired by excitatory (*black*) and inhibitory (*gray*) neurons in the initial 10 s of a simulation. Inhibitory neurons were suppressed at the 4th s, followed by the synchronized burst firing of excitatory neurons. Panels *b* and *c* display the numbers of APs fired by excitatory neurons in 1-s-long periods at the 12th and 69th s of the simulation, respectively. Note the different scales in the panels. (*d*) Pattern of burst frequencies in a population of excitatory neurons obtained in a 300-s-long simulation of epileptiform activity. Points represent instant frequencies obtained by taking the inverse of burst-to-burst intervals in 81 neurons. The onset of bursting activity was positioned at $t = 0$. For comparison, the top-right inset (control) shows a pattern of AP frequencies in neurons obtained in a simulation when inhibition was present. In the control simulation, the strength of the inhibitory synapses was adjusted to the level that prevents the occurrence of bursts in neurons. Parameters: $[B]_i^{total} = 50\ \mu M$, $[Bs]_i^{total} = 1200\ \mu M$, $\tau_{sAHP} = 200–500$ ms (*a–c*); all other parameters as in the Supporting Material sections A–D.

control simulation, neurons receive robust inhibitory input and fire mostly single APs and only sporadically bursts. Initially, these APs are fired at nearly random intervals in the range of 100 ms to 1 s (1–10 Hz firing). Later, the pattern is dominated by APs firing in the range of 1–5 Hz.

The mechanism of the decline of burst frequency was investigated by analyzing $[Ca^{2+}]_i$ time courses and membrane current transients in a cell model. Simulated $[Ca^{2+}]_i$ time courses in the outermost shell positioned at 0.5 μm underneath the membrane of a 20-μm-radius spherical neuron are plotted in Fig. 2 *a*. The bottom panel shows a detailed comparison of $[Ca^{2+}]_i$ time courses between two consecutive bursts occurring at 3 s and 57 s after the onset of the simulated epileptiform activity. These $[Ca^{2+}]_i$ time courses correspond to 7.5 and 3 Hz burst patterns, respectively. The burst-to-burst intervals are 132 and 336 ms, respectively. The $[Ca^{2+}]_i$ baseline (i.e., $[Ca^{2+}]_i$ before the burst onset) in the outermost shell at the 3rd s (7.5 Hz pattern) is 68 nM, whereas at the 57th s (3 Hz pattern) it is ~78 nM. At the 7.5 Hz and 3 Hz burst patterns, the maximal amplitude of $[Ca^{2+}]_i$ reaches a peak at 200 nM and 250 nM, respectively. The rate at which $[Ca^{2+}]_i$ decreases in the outermost shell between two consecutive bursts is higher at the 7.5 Hz burst pattern than at the 3 Hz pattern. The top and middle panels in Fig. 2 *a* show a comparison of membrane voltages. The enlargement (*middle panel*) shows that the larger membrane hyperpolarization after burst occurs at the 3 Hz pattern.

Fig. 2 *b* (*top panel*) shows a comparison of I_{Ca} current transients occurring at the 3rd (7.5 Hz pattern) and 57th (3 Hz pattern) seconds of the activity. The amplitude of I_{Ca} current at the 3 Hz burst pattern reaches a peak at 15–20% larger values compared to the 7.5 Hz pattern.

A similar comparison of I_{sAHP} current transients is shown in the middle and bottom panels Fig. 2. The 3 Hz burst pattern is associated with larger increases in the amplitude of I_{sAHP} current after each AP compared to the 7.5 Hz pattern.

Fig. 2 *c* illustrates the time courses of simulated free ($[B]_i$) and Ca-bound ($[BCa^{2+}]_i$) mobile buffer concentrations occurring at 0.5 μm underneath the membrane. $[B]_i$ and $[BCa^{2+}]_i$ time courses are shown, between the same two consecutive bursts as in Fig. 2, *a* and *b*. The baseline level of $[B]_i$ associated with the 7.5 Hz burst pattern is 46.75 μM and is ~0.25 μM larger than the $[B]_i$ baseline level seen at the 3 Hz pattern. The 3 Hz burst pattern is associated with significantly larger $[B]_i$ changes. The drop in $[B]_i$ after a single AP is ~0.5–0.7 μM, and is ~0.2 μM (40%) larger than the analogous $[B]_i$ drop seen at the 7.5 Hz burst pattern. The 7.5 Hz burst pattern is characterized by a lower $[BCa^{2+}]_i$ baseline level (3.2 μM)

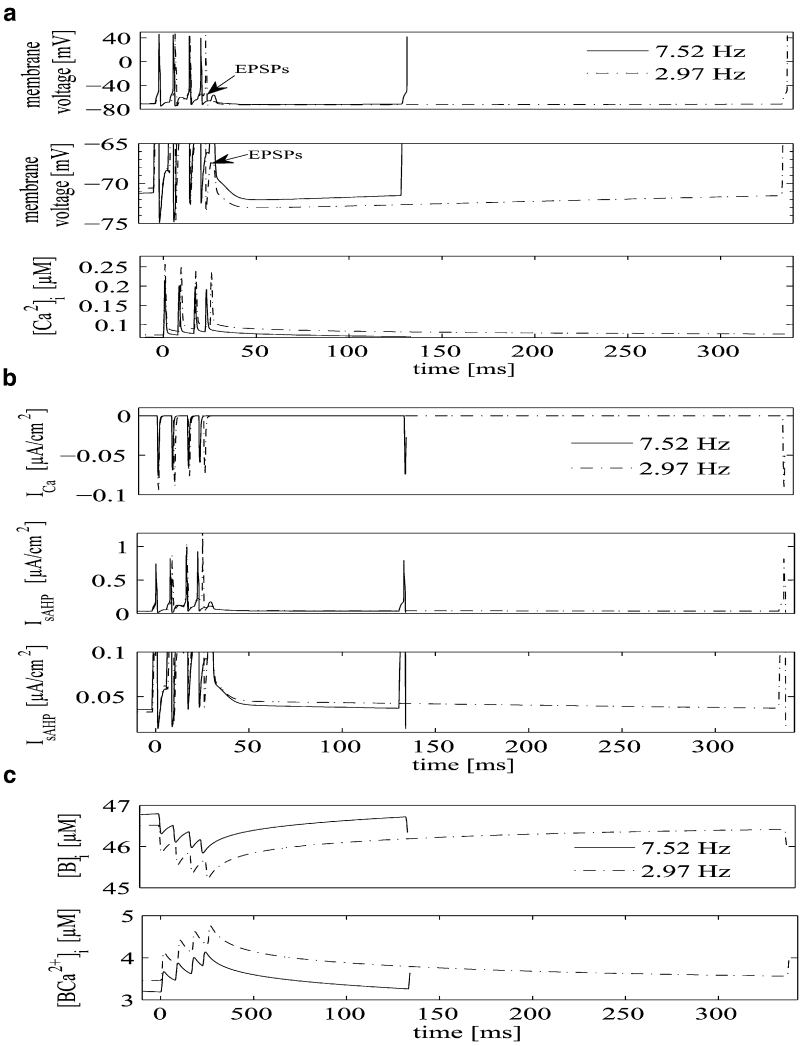

FIGURE 2 (*a*) Comparisons of voltage traces (*top* and *middle*) and $[Ca^{2+}]_i$ time courses (*bottom*) corresponding to the 7.5 Hz (*line*) and 3 Hz (*dashed*) burst patterns. Voltage and $[Ca^{2+}]_i$ time courses are plotted between two consecutive bursts. $[Ca^{2+}]_i$ was obtained in the outermost shell at 0.5 μm underneath the membrane of a 20-μm-radius spherical neuron. These voltage and $[Ca^{2+}]_i$ transients occur at the 3rd and 57th s, respectively, of the simulated epileptiform activity. The termination of bursts is accompanied by EPSPs that follow AP trains, which are shown in the top and middle (*enlargement*) panels. (*b*) Comparisons of I_{Ca} (*top*) and I_{sAHP} (*middle*) current transients occurring between two consecutive bursts at the 3rd and 57th s of the simulated epileptiform activity and corresponding respectively to the 7.5 Hz and 3 Hz burst frequency patterns. The bottom panel is an enlargement of the middle panel. (*c*) Comparisons of $[B]_i$ and $[BCa^{2+}]_i$ time courses between two consecutive bursts obtained at the 3rd (7.5 Hz burst pattern) and 57th (3 Hz pattern) seconds of the simulation. $[B]_i$ and $[BCa^{2+}]_i$ time courses were measured in the outermost shell positioned at 0.5 μm underneath the membrane of a 20-μm-radius spherical neuron. All parameters as in Fig. 1.

and is ~0.25 μM lower than the $[BCa^{2+}]_i$ baseline level seen at the 3 Hz burst pattern. The amplitude of the $[BCa^{2+}]_i$ peak after a single AP is in the range of 0.5–07 μM at the 3 Hz burst pattern and is ~40% larger than the amplitude of the $[BCa^{2+}]_i$ peak observed at the 7.5 Hz pattern.

$[Bs]_i$ and $[BsCa^{2+}]_i$ change very slowly (on a timescale of seconds) in neurons, and they remain almost unchanged throughout the time course of a single burst. In the outermost shell, the 7.5 Hz burst pattern is characterized by an ~3.5% higher level of $[Bs]_i$ (1105.6 μM) compared to the 3 Hz burst pattern (1066.4 μM). The 3 Hz burst pattern in turn is associated with an almost 40% larger $[BsCa^{2+}]_i$ level (133.5 μM) compared to the 7.5 Hz pattern (94.6 μM; data not shown).

We next focused on analyzing $[Ca^{2+}]_i$ transients in spherical neurons under the conditions of a prolonged recurrent neuronal burst firing. Our goal was to provide a quantitative description of $[Ca^{2+}]_i$ dynamics in a neuron throughout the entire period of the simulated ictal activity. Fig. 3 illustrates $[Ca^{2+}]_i$ dynamics obtained at 0.5 and 5 μm underneath the membrane of a 20-μm-radius spherical neuron in a 300-s-long simulation. The onset of recurrent bursting is positioned at $t = 0$. The $[Ca^{2+}]_i$ dynamics has at least three components occurring on different timescales. The largest and fastest increases in the $[Ca^{2+}]_i$ time courses occur in the outermost shell at 0.5 μm underneath the membrane (Fig. 3 *a*). Momentary $[Ca^{2+}]_i$ increases to 0.2–0.3 μM occur coincidently with APs fired by the neuron. The average $[Ca^{2+}]_i$ elevation ($\Delta[Ca^{2+}]_i$) evoked by a single AP in the outermost shell is ~4–6 nM. Because Ca^{2+} is heavily buffered and Ca^{2+} influx is in the outermost shell, both the amplitude of $[Ca^{2+}]_i$ peaks and $\Delta[Ca^{2+}]_i$ show large attenuations in subsequent shells as the distance from the cell surface increases. The $[Ca^{2+}]_i$ peaks associated with AP trains and the resulting $\Delta[Ca^{2+}]_i$ elevations are followed by a slow component in which $[Ca^{2+}]_i$ decreases slowly over 50–100 ms until the next burst is initiated. Fig. 3 *b* shows the third component, which occurs on a timescale of minutes, with the fast and slow $[Ca^{2+}]_i$ transients components superimposed on it. It is characterized by a slow increase in $[Ca^{2+}]_i$ baseline level, which reaches a plateau between 200 and 300 s. The panel shows an enlargement illustrating $[Ca^{2+}]_i$ changes occurring in shells positioned at 0.5 and 5 μm underneath the membrane.

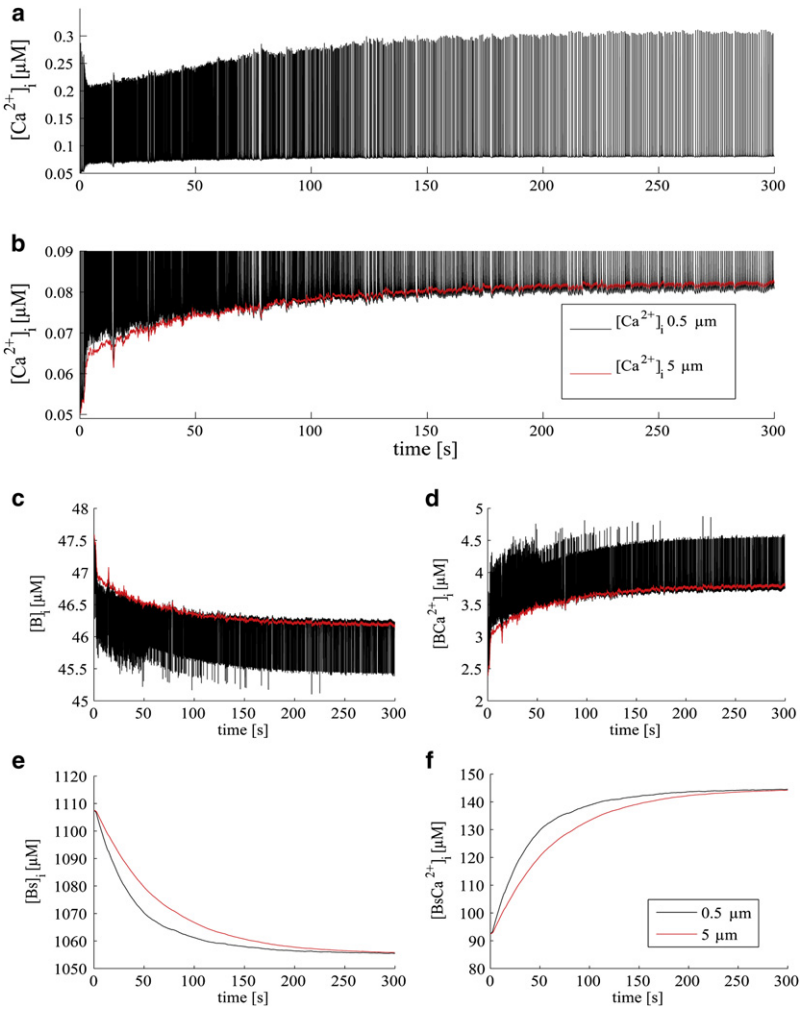

FIGURE 3 Calcium dynamics in a 20-μm-radius spherical neuron under conditions of prolonged recurrent neuronal burst firing. (*a*) $[Ca^{2+}]_i$ dynamics obtained in a shell positioned at 0.5 μm underneath the membrane throughout the 300-s long period of the simulated epileptiform activity. (*b*) Enlargement of panel a illustrates a very slow component of $[Ca^{2+}]_i$ dynamics in shells positioned at 0.5 μm (*black*) and 5 μm (*red*) underneath the membrane characterized by the slow increase with subsequent saturation in $[Ca^{2+}]_i$ baseline level that is associated with recurrent neuronal bursting. A recurrent bursting leads to $[Ca^{2+}]_i$ baseline increase to ~80 nM (from 50 nM). (*c*) Changes in the concentration of mobile buffers ($[B]_i$) in shells positioned at 0.5 (*black*) and 5 μm (*red*) underneath the membrane during simulated epileptiform activity. (*d*) $[BCa^{2+}]_i$ changes in shells positioned at 0.5 (*black*) and 5 μm (*red*) underneath the membrane. Panels *e* and *f* show free and Ca-bound fixed buffer concentration changes ($[Bs]_i$ and $[BsCa^{2+}]_i$, respectively) in analogous shells at 0.5 (*black*) and 5 μm (*red*) underneath the membrane. $[Bs]_i$ shows a hyperbolic decrease over the time course of tens of seconds to minutes. All parameters as in Fig. 1.

A few seconds after the onset of the recurrent bursting, the $[Ca^{2+}]_i$ baseline level is typically 1–2.5 nM higher in the outermost shell than in the shell positioned at 5 μm underneath the membrane. It remains greater in the outermost shell for ~60 s after the onset of the recurrent bursts, but the $[Ca^{2+}]_i^{0.5\mu m} - [Ca^{2+}]_i^{5\mu m}$ difference slowly decreases; ~65 s after the onset of epileptiform activity, equal $[Ca^{2+}]_i$ baseline levels (75 nM) are seen in both shells. From ~70th s of the simulation, the $[Ca^{2+}]_i^{5\mu m} - [Ca^{2+}]_i^{0.5\mu m}$ difference begins to increase and a larger $[Ca^{2+}]_i$ baseline is found in the shell positioned at 5 μm underneath the membrane rather than in the outermost shell. At the end of the simulation ($t = 300$ s), the $[Ca^{2+}]_i$ baseline level in the outermost shell is ~80 nM and is typically 1.25 nM lower than $[Ca^{2+}]_i$ in the shell positioned at 5 μm underneath the membrane.

The mechanism of the initial slow increase and subsequent plateau of the $[Ca^{2+}]_i$ baseline level was investigated by analyzing the redistribution of B inside neurons, and by examining changes in $[Bs]_i$. Fig. 3 illustrates changes in $[B]_i$ (panel *c*) and $[BCa^{2+}]_i$ (panel *d*) in shells positioned at 0.5 and 5 μm underneath the membrane. Throughout the duration of the simulated epileptiform activity, the baseline level of $[B]_i$ in the outermost shell decreases slowly from 47 to 46.25 μM (1%), whereas the concentration of $[BCa^{2+}]_i$ increases from ~3 to 3.75 μM. Initially, the baseline level of $[B]_i$ in the outermost shell is ~0.12 μM lower compared to $[B]_i$ in the shell positioned at 5 μm underneath the membrane. The difference in baseline levels $[B]_i^{5\mu m} - [B]_i^{0.5\mu m}$ decreases over the time course of the simulated activity. At ~65th s, equal $[B]_i$ baseline levels (46.5 μM) are seen in both shells. Beginning at 70–80 s, the $[B]_i$ baseline in the outermost shell is higher than $[B]_i$ in shells positioned at 5 μm. Finally, at the end of the simulation ($t = 300$ s), the $[B]_i$ baseline in the outermost shell is 46.25 μM and is ~0.05 μM higher than $[B]_i$ in the shell positioned at 5 μm underneath the membrane.

The changes in the concentration of $[Bs]_i$ and $[BsCa^{2+}]_i$ at 0.5 and 5 μm underneath the membrane are illustrated in Fig. 3, *e* and *f*. $[Bs]_i$ shows a hyperbolic decrease in the time course of the simulated epileptiform activity. The concentration of $[Bs]_i$ decreases from 1120 to 1060 μM (5%), whereas the concentration of $[BsCa^{2+}]_i$ increases from 90 to 144 μM. The rate of $[Bs]_i$ decrease is not uniform inside a cell; it varies from shell to shell and changes throughout the duration of the simulated epileptiform activity. Initially, the highest rate of

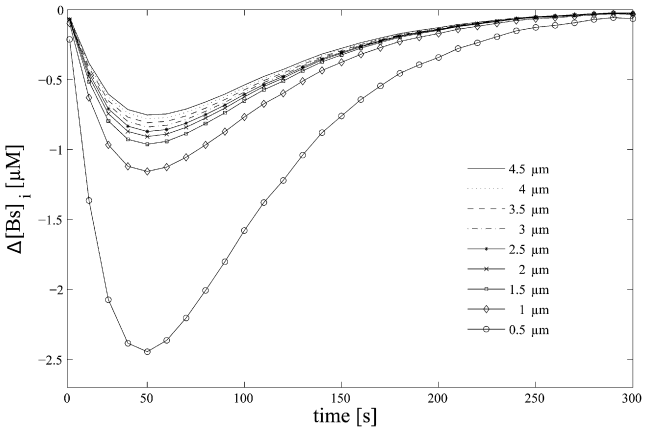

FIGURE 4 Spatiotemporal $[Bs]_i$ gradients (in a radial direction) in a 20-μm-radius spherical neurons model formed throughout the duration of the simulated 300-s-long epileptiform activity. $\Delta[Bs]_i$ was calculated by taking $[Bs]_i^j$ in a given j shell (starting from the outermost shell) and subtracting $[Bs]_i^{j-1}$ from the next underneath shell. A homogeneous $[Bs]_i$ distribution inside the cell model was assumed. All parameters as in Fig. 1.

$[Bs]_i$ decrease is seen in the outermost shell, and the lowest is seen in the shell positioned at 5 μm underneath the membrane. After ~40 s, the fastest rate of $[Bs]_i$ decrease is seen at 5 μm underneath the membrane, and the slowest is observed in the outermost shell.

The variation in $[Bs]_i$ distribution inside a cell results in the formation of spatiotemporal $[Bs]_i$ gradients throughout the duration of the simulated activity. To illustrate this, $\Delta[Bs]_i$ were calculated by subtracting $[Bs]_i^j$ in a given j shell (starting from the outermost $j = 9$) from $[Bs]_i^{j-1}$ in the next underneath shell. The resulting $[Bs]_i$ gradients occurring in a cell model in a radial direction at different distances relative to the membrane position are plotted in Fig. 4. The largest $\Delta[Bs]_i$ occurs at 0.5 μm underneath the membrane. There are two phases in the $\Delta[Bs]_i$ plot. The first phase lasts for ~40 s and is characterized by $\Delta[Bs]_i$ growth (absolute value). In the second phase, $\Delta[Bs]_i$ gradually and slowly decreases until it reaches its equilibrium state. The growth and decline phases in the $[Bs]_i$ gradient plot are correlated with B redistribution inside the cell (Fig. 3 *c*).

The growth phase corresponds to the initial period, when $[B]_i$ is lower in the outermost shell than in the remaining shells positioned deeper underneath the membrane. The decline phase corresponds to the later period (>60–70 s) when higher $[B]_i$ is found in shells positioned closer relative to the membrane than in deeper shells.

The effect of varying Ca^{2+} mobility on the formation of $[Bs]_i$ gradients inside a cell is illustrated in Fig. 5 *a*, which shows $\Delta[Bs]_i$ obtained at 0.5 μm underneath the membrane. It can be seen that increasing the Ca^{2+} diffusion coefficient reduces the $\Delta[Bs]_i$ peak but has no effect on the duration of $\Delta[Bs]_i$ growth and reduction phases. The formation of $\Delta[Bs]_i$ as functions of B mobility and affinity are illustrated in Fig. 5, *b* and *c*. Varying both the diffusion coefficient (panel *b*) and the dissociation constant K_B (panel *c*) of B has the expected larger effect on the duration and amplitude of $\Delta[Bs]_i$ transients. A 10-fold decrease in B mobility (from 1.0 to 0.1 $\times$ 10^6 cm^2/s) results in an ~75% increase in the amplitude of the $\Delta[Bs]_i$ peak in the outermost shell. It can be also seen that the reduction phase of the $\Delta[Bs]_i$ transient becomes longer as the mobility of B decreases. The affinity of B has a slightly more prominent effect on the duration of $\Delta[Bs]_i$ transients. The results of variations in B binding forward and backward rates on $\Delta[Bs]_i$ are illustrated in Fig. 5 *c*. The high affinity of the mobile buffers (K_B = 0.5 μM, $k_+ = 2\times10^5\ M^{-1}\cdot ms^{-1}$) is associated with the lower amplitude of the $\Delta[Bs]_i$ peak, and also with the shorter duration of the $\Delta[Bs]_i$ growth and reduction phases compared to

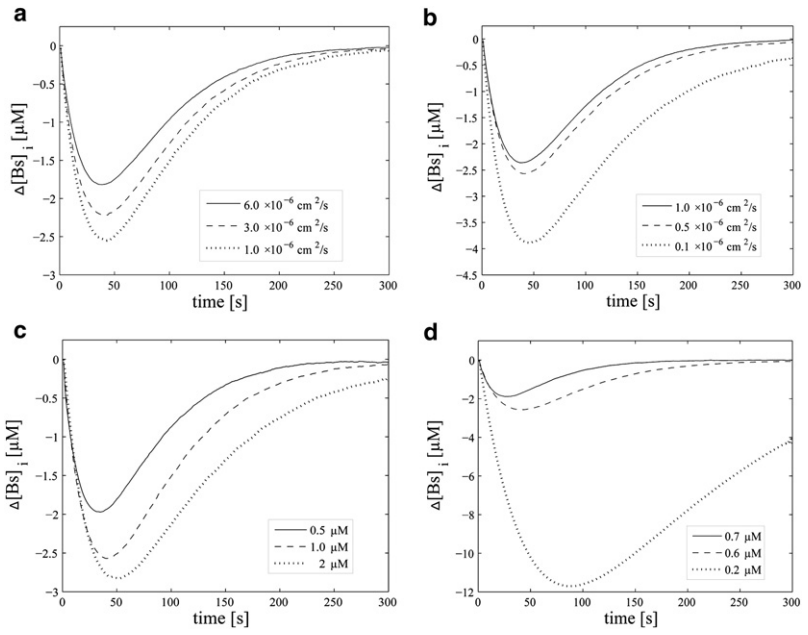

FIGURE 5 (*a*) Effect of varying Ca^{2+} mobility on $\Delta[Bs]_i$. An increase in Ca^{2+} mobility reduces the $\Delta[Bs]_i$ peak but has no effect on the duration of $\Delta[Bs]_i$ transients. (*b*) Effect of varying B mobility on $\Delta[Bs]_i$. (*c*) Effect of varying B affinity on $\Delta[Bs]_i$. Micromolar concentration and high affinity of B produce a larger effect on the duration and amplitude of $\Delta[Bs]_i$ transients despite the lower than Ca^{2+} mobility of B. (*d*) Effect of varying Bs affinity on $\Delta[Bs]_i$. Each curve was obtained by averaging data from eight neurons. $\Delta[Bs]_i$ was calculated 0.5 μm underneath the membrane (*outermost shell*) of a 20-μm-radius cell model. All parameters as in Fig. 1.

$\Delta[Bs]_i$ transients obtained for low B affinity ($K_B = 2\ \mu M$, $k_+ = 0.5 \times 10^5\ M^{-1} \cdot ms^{-1}$). The longer duration of $\Delta[Bs]_i$ transients in the latter results from the larger amount of free Ca^{2+}. With a low B affinity, the Ca^{2+} clearance depends more on slow mechanisms (binding to Bs, diffusion, and efflux).

The effect of varying Bs affinity on $\Delta[Bs]_i$ transients is illustrated in Fig. 5 *d*. It can be seen that Bs affinity may have a significant effect on $\Delta[Bs]_i$. A high Bs affinity (0.2 μM, $k_+ = 50\ M^{-1} \cdot ms^{-1}$) is associated with the generation of a large spatial Bs gradient in the outermost shell in the model ($\Delta[Bs]_i$ peaks at 12 μM). A large amplitude of the $\Delta[Bs]_i$ peak can be expected with high Bs affinity because Ca^{2+} influx is present in the outermost shell and Bs is defined as a fixed buffer. Both the duration and amplitude of the $\Delta[Bs]_i$ transients decrease as Bs affinity decreases.

As indicated by Fig. 5, *b–d*, an increase in the $\Delta[Bs]_i$ peak and duration can result from either an increase in Bs concentration or a decrease in B concentration. The effect of variations of total concentrations of B ($[B]_i^{total}$) and Bs ($[Bs]_i^{total}$) on the formation of Bs gradients in a cell is illustrated in Fig. 6. Indeed, larger $[Bs]_i^{total}$ values are associated with a larger amplitude of the $\Delta[Bs]_i$ peak, which is consistent with the results of the Bs affinity studies shown in Fig. 5 *d*. An increase in $[B]_i^{total}$ has the opposite effect on $\Delta[Bs]_i$ peak and duration, which is not surprising given that B is essential for redistributing Ca^{2+} in a cell. The effect of varying $[B]_i^{total}$ on $\Delta[Bs]_i$ is consistent with the results of the B mobility (Fig. 5 *b*) and B affinity (Fig. 5 *c*) studies.

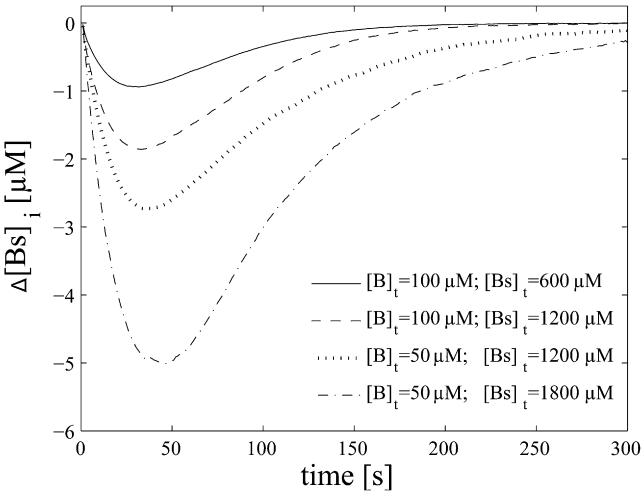

FIGURE 6 Effect of changing $[B]_i^{total}$ and $[Bs]_i^{total}$ on $[Bs]_i$ gradients. A comparison of $[Bs]_i$ gradient plots obtained in a four different simulation runs, each with a different $[B]_i^{total}/[Bs]_i^{total}$ ratio, is shown. Each curve was obtained by averaging data from eight neurons. $\Delta[Bs]_i$ was calculated 0.5 μm underneath the membrane of a 20-μm-radius cell model. The time window of the frequency decline (i.e., the duration) can be predicted based on the $[B]_i^{total}/[Bs]_i^{total}$ ratio. Parameters as in the Supporting Material sections A–D.

DISCUSSION

In this network model, we simulate epileptiform activity in a disinhibited neuronal network in which continuous repetitive neuronal bursting activity arises from mutual neuronal excitation in the network. After the inhibitory neurons are suppressed, bursts of APs arise simultaneously in a population of excitatory neurons. This is achieved by adjusting the strength of the excitatory synapses to a level that allows burst spreading from pre- to postsynaptic neurons throughout the network. Bursts are initiated in local recurrent excitatory synaptic pathways by random APs delivered to the selected neurons located in the center of the network (to ensure that the frequencies of burst in the network do not follow the frequency of randomly delivered APs, Ca^{2+} dynamics is not modeled in these neurons). Once initiated locally, they spread rapidly to remote neurons in the network via long-range excitatory synaptic pathways and are maintained in remote areas via local recurrent excitatory synaptic pathways.

The synchrony in the network is characterized by the simultaneous occurrence of bursts of APs in a population of excitatory neurons. Synchronization implies that during burst periods of 50–100 ms, bursts in any two neurons will occur within tens of milliseconds of one another. The synchrony appears to not be affected by network boundary conditions. In a network with open boundary conditions, a reflection effect on the periphery of the model can be expected. In fact, suppression of random APs delivered to neurons results in the cessation of activity in the entire network. This can be explained by the imposed strength of the synaptic contacts, network long-range wiring, and the lack of inhibition. Strong long-range synaptic connections, along with a suppressed inhibitory drive, prevent the occurrence of local synchronization on edges in a network. The boundary effect is evident in networks with local connectivity and when inhibition is present.

When inhibition is absent, termination of synchronous bursts in a network results from activation of the I_{sAHP} current in neurons. The amplitude of I_{sAHP} increases with each AP fired by a neuron, and thus this current becomes prominent at the end of each burst. It can be seen in Fig. 2 *a*, where burst termination in a neuron is accompanied by excitatory postsynaptic potentials (EPSPs) that follow the APs train. Normally, these EPSPs have sufficient amplitude to induce an AP, but are unable to do so because of the increased amplitude of I_{sAHP} (Fig. 2 *b*).

Abel et al. (4) investigated the effects of recent discharge on $[Ca^{2+}]_i$ and AHP activation in neocortical pyramidal neurons. Their data suggest that the activation of sAHP channels requires an elevation of $[Ca^{2+}]_i$ in the cytoplasm, rather than at the membrane. This observation is consistent with the modeling approach we adopted, in the sense that our model requires a cytoplasmic intermediate to reproduce interactions between $[Ca^{2+}]_i$ and the sAHP channels. The results of our studies indicate that the elevation of $[Ca^{2+}]_i$ baseline in

shells, but not the amplitude of momentary $[Ca^{2+}]_i$ peaks, affects the way in which recurrent bursts in neurons are terminated by the I_{sAHP}.

One of the consequences of burst termination by sAHP is that the number of APs fired by neurons within a single burst train varies throughout the duration of the simulated activity. Soon after the onset of recurrent bursting, neurons typically fire 4–5 APs per burst, and later this number decreases to 1–2 APs. This is because the mechanism of burst termination is affected by the increasing baseline level of $[Ca^{2+}]_i$ in neurons (i.e., in the range of 70–90 nM). The I_{sAHP} current is modeled with a sigmoidal activation function that depends on $[Ca^{2+}]_i$ with a midpoint at 140 nM. The increase in $[Ca^{2+}]_i$ baseline level may therefore affect the length of bursts by changing the number of APs fired by a neuron within a single burst. An increase in $[Ca^{2+}]_i$ baseline level from 70 to 80 nM results in an increase of activation variable w_{sAHP} from 0.06 to 0.098 (39%), whereas τ_{sAHP} decreases from 188 to 180 ms. In the model, this corresponds to ~4 APs/burst occurring at $[Ca^{2+}]_i = 70$ nM and 1–2 APs/burst at 80 nM, respectively. The sAHP activation time τ_{sAHP} alone has little effect on the occurrence of bursting in neurons. The change in τ_{sAHP} resulting from the $[Ca^{2+}]_i$ baseline increase is not large. Throughout the time course of the simulated bursting period, the $[Ca^{2+}]_i$ baseline remains in the range of 50 to 100 nM, and the τ_{sAHP} typically varies between 170 and 190 ms. An increase in τ_{sAHP} has a minor effect on bursting. A small (7%) increase in the $\Delta[Bs]_i$ peak (data not shown) is observed when τ_{sAHP} is modeled between 200 and 500 ms, and no change in the $\Delta[Bs]_i$ peak is seen when τ_{sAHP} is between 500 and 1000 ms. This behavior can be explained by the change in the affinity of simulated sAHP channels. An increase in τ_{sAHP} shifts the midpoint of the sAHP activation function w_{sAHP} toward lower $[Ca^{2+}]_i$ values (higher affinity).

The I_{sAHP} is modeled with half-activation between 100 and 300 nM. In this range, the affinity of sAHP channels to Ca^{2+} ions is not critical for the occurrence of synchronous bursting and for the mechanism of burst termination by the I_{sAHP}. However, varying the midpoint for sAHP activation can affect how fast (after suppression of inhibition) synchronous bursting in a network occurs. When sAHP is modeled with relatively low affinity (half-activation at 249 nM), bursting activity in a network is fully developed 30 s after the suppression of inhibition. In contrast, with high sAHP affinity (half-activation at 140 nM), bursting activity typically occurs after 5–10 s. Before the onset of bursting and after suppression of inhibition, neurons exhibit continuous firing. This firing results from the fact that an increase of the sAHP half-activation point above 230 nM produces very weak spike frequency adaptation in neurons. Overall shifting of the $[Ca^{2+}]_i$ midpoint for sAHP channel activation toward higher $[Ca^{2+}]_i$ (lower affinity) delays the onset of synchronous bursting in a network.

In simulations, the Na^+/Ca^{2+} exchanger has a maximal rate of Ca^{2+} removal of 2 pmol/cm^2/s. This value is similar to the rate reported for squid axons (5) and to those used in other cell models (6,7). Assuming this rate of Ca^{2+} removal, the electrogenic current generated by Na^+/Ca^{2+} exchanger in the model is in a low nA/cm^2 range (sub-pA) and its contribution to the membrane polarization is not significant. This seems likely given that the maximal rate of the Na^+/Ca^{2+} exchanger in neurons is typically lower by a factor of 10^3 than that of ion-conductive channels (8). Furthermore, even a 10-fold increase in the value of k_{NaCa} (scaling factor) in the model does not make I_{NaCa} strong enough to counterbalance the membrane hyperpolarization elicited by sAHP. Such an increase in the Na^+/Ca^{2+} transport rate, however, has an effect on $[Ca^{2+}]_i$ transients in the outermost shell, including a reduction in the amplitude of $[Ca^{2+}]_i$ peaks and lowering of the $[Ca^{2+}]_i$ baseline level in the outermost shell. An increased Ca^{2+} efflux via the Na^+/Ca^{2+} exchanger affects the rate of change and range of burst frequencies that are observed in the model. This includes an increase of the bottom frequency in the pattern of frequency decline shown in Fig. 1 *d*. A 10-fold increase in the value of k_{NaCa} causes the burst frequency to decline to 4.5 Hz, with a rate of frequency decline of ~2 Hz/min (versus 2 Hz and 4 Hz/min in Fig. 1 *d*).

This simulation study showed the existence of a very slow component in $[Ca^{2+}]_i$ dynamics throughout the duration of the simulated epileptiform activity. We suggest that a similar component may appear in dynamics of $[Ca^{2+}]_i$ in neurons in brain throughout the duration of the ictal period. This slow component is characterized by a gradual increase and subsequent plateau in the $[Ca^{2+}]_i$ baseline level in neurons. The initial slow rise in the $[Ca^{2+}]_i$ baseline level may be explained based on the characteristics of the endogenous buffer systems in cells. $[Ca^{2+}]_i$ in the cell is largely regulated by fast and slow buffers (~98% of entering Ca^{2+} is bound to these buffers). These two buffer systems differ considerably in speed, capacity, and mobility. The Ca^{2+} clearance process will be altered if the concentrations of both slow and fast Ca^{2+} buffers in their free form change over the time course of the recurrent neuronal bursting. This is likely to occur, given that Ca^{2+} influx is solely present in the outermost shell, and the two Ca^{2+} buffer systems operate continuously at different speeds throughout the duration of the epileptiform activity, which lasts for 3–4 min.

In our spherical cell model studies, $[Bs]_i$ shows a hyperbolic decrease over the time course of tens of seconds to minutes (Fig. 3 *e*), with a rate that is not spatially uniform inside a cell. These various rates of $[Bs]_i$ decrease in cells can be explained on the basis of the speed of Ca^{2+} and B diffusion and the rate of Ca^{2+} extrusion. Extrusion and diffusion are slow mechanisms, and they are unable to transport the unbound portion of Ca^{2+} ions from the outermost shell at the same rate at which free Ca^{2+} increases in a cell during recurrent bursting. The excess is bound to Ca^{2+} buffers. Therefore, the fastest rate of $[Bs]_i$ decrease is seen in the outermost shell. The nonuniform rate of $[Bs]_i$ decrease leads

to the formation of a spatial gradient in Bs concentration (assuming that Bs is uniformly distributed inside a cell). This spatial $[Bs]_i$ gradient, apart from directly affecting the $[Ca^{2+}]_i$ level, affects the concentration and spatial distribution of B in both free and Ca-bound forms (Fig. 3, *c* and *d*). The formation of spatial $[Bs]_i$ gradients is therefore attributed to the slow redistribution of $[B]_i$ and $[BCa^{2+}]_i$ inside the cell acting against these gradients until new equilibrium points for $[Bs]_i$, in the shells are reached (Fig. 3 *e*).

Notably, the I_{sAHP} current in neurons also controls how fixed and mobile Ca^{2+} buffer systems respond to the occurrence of recurrent bursting. The increase in I_{sAHP} amplitude resulting from the $[Ca^{2+}]_i$ baseline rise in neurons reduces the amount of Ca^{2+} that enters into neurons by increasing the interburst intervals in neurons. $[B]_i$ and $[Bs]_i$ characteristics would differ from those shown in Fig. 3, *c* and *e*, if I_{sAHP} were not simulated in neurons. The behavior of the Ca^{2+} clearance system can be understood more easily by analyzing the evolution of the system in the three-dimensional phase space illustrated in Fig. 7. The phase space is spanned by the slowly changing variables $[Bs]_i$, $[B]_i$, and $[Ca^{2+}]_i$. For simplicity, we will assume that the system is in equilibrium before the withdrawal of inhibition (i.e., no activity in a network). For a neuron at rest, the values in the phase space are $[Ca^{2+}]_i = 50.4$ nM, $[B]_i = 47.58\ \mu$M, and $[Bs]_i = 1107.47\ \mu$M. After the onset of recurrent bursting, the system enters into the oscillatory state (orbits in the phase space) each time a cell fires trains of APs. The trajectories are plotted in the phase space diagram in Fig. 7. $[Bs]_i$, $[B]_i$, and $[Ca^{2+}]_i$ vary in a neuron throughout the duration of the simulated epileptiform activity, and this is associated with a series of orbits and a slow transition of the system in phase space (the arrow shows the direction of the evolution). The red color illustrates the space the system occupies in the initial 5 s of the simulation starting from the 10th s after the onset of recurrent bursting. The yellow indicates the 5 s of the simulation beginning from the 175th s after the onset of recurrent bursting. The relatively large volume (*red*) that the system occupies in the initial 10–15 s period versus the small volume (*yellow*) in the 175–180 s period indicates that the trajectories converge to a stable attractor, where the system exhibits more complex than limited cycle behaviors. Similar system behaviors can be anticipated based on Fig. 3. All plotted variables do not change significantly starting from $t = 200$ s. Both the $[B]_i$ and $[Bs]_i$ baselines in Fig. 3, *c* and *e*, as well as the $[Ca^{2+}]_i$ baseline (Fig. 3 *b*) slowly approach their asymptotic values.

Each burst fired by a cell is accompanied by a $[Ca^{2+}]_i$ baseline level buildup. A similar buildup in the $[Ca^{2+}]_i$ baseline was previously observed in a model of bullfrog sympathetic ganglion neurons (9). The somatic $[Ca^{2+}]_i$ increases were contingent on the number of synaptic inputs (or fired APs) delivered to neurons during 0.5 s of stimulation. The observed $[Ca^{2+}]_i$ buildup was relatively independent of input frequency in the range of 10–50 Hz. These findings are in

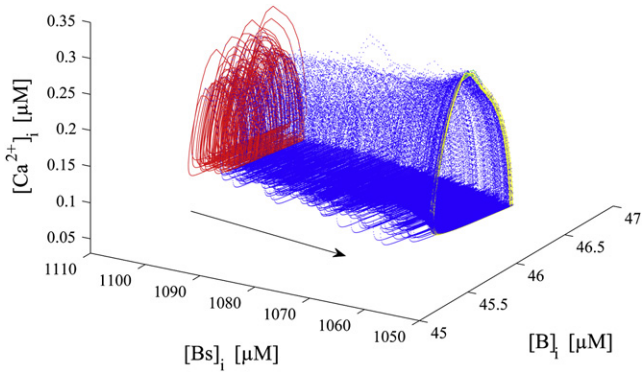

FIGURE 7 Phase-space diagram of slowly changing $[Bs]_i$, $[B]_i$, and $[Ca^{2+}]_i$ variables throughout 180 s of the simulated epileptiform activity. The trajectories describe the evolution of the system from the initial state at rest. The oscillatory behaviors correspond to periods in which a cell fires bursts of APs. The plotted orbits represent ~570 bursts separated by interburst intervals. The arrow indicates the direction of orbit evolution. Red and yellow colors are used to indicate orbits corresponding to the simulation periods 10–15 s and 75–180 s, respectively. All parameters as in Fig. 1.

agreement with the $[Ca^{2+}]_i$ buildup we observed during burst periods in our model, where the average $[Ca^{2+}]_i$ elevation is 4–6 nM/AP.

Throughout the duration of the simulated epileptiform activity, the $[Ca^{2+}]_i$ baseline levels in cells slowly increase. Similar slow $[Ca^{2+}]_i$ increases were observed experimentally in molluscan neurons in response to step depolarizations (10) and in bullfrog sympathetic neurons (11) following AP trains. In molluscan neurons, Ca^{2+} dye signals approach a plateau at pulse durations longer than 10 s. These data suggest that the Ca^{2+} clearance system in an isolated neuron may react faster to activation. However, this faster response can result from a different protocol used for cell activation. In isolated neurons that are mostly activated by current injection or repetitive synaptic stimulation, the response of the Ca^{2+} clearance systems may be more rapid than the response of these systems in network assemblies, where activation primarily results from synaptic interactions. In our model, neurons receive periodically quasirepetitive synaptic inputs, which are associated with the occurrence of bursts in the network. The frequency of burst occurrence in the network is in the range of 2–8 Hz, which might explain the observed slower $[Ca^{2+}]_i$ buildup.

These analyses helped us identify what we believe is a novel mechanism of neuronal-excitability regulation that occurs in conditions of prolonged and recurrent neuronal bursting in a disinhibited neuronal network. This type of regulation may occur in real neuronal ensembles throughout the duration of seizure or epileptiform activity. It is made possible by the interactions of two cellular mechanisms: 1), Ca-dependent K^+ channels regulating membrane excitability; and 2), Ca^{2+} clearance systems in neurons. A slowly increasing $[Ca^{2+}]_i$ baseline level in cells results in a decrease in neuronal membrane excitability, mostly by activating the

Ca-dependent K^+ channels. The decrease in neuronal membrane excitability is reflected in an increase of the interburst intervals during the simulated epileptiform activity. The resulting changes in the behavior of neurons affect the entire dynamics and evolution of the simulated epileptiform activity in the network. The increasing interburst intervals in neurons reduce the amount of Ca^{2+} that enters into neurons in a time unit. As a consequence, $[Ca^{2+}]_i$ in neurons is partially saturated at certain levels that are sufficient to prevent neuronal bursting in a network, instead of increasing to a high toxic level. The described mechanism represents a type of regulatory mechanism that affects network excitability behavior. We emphasize that it arises slowly throughout synaptic interactions in a network and is rather unlikely to occur in isolated neurons. Therefore it can serve, and might be conceptually considered, as a network safety mechanism to prevent excessive and uncontrolled neuronal firing resulting from the lack of inhibition, or after the acute suppression of inhibitory neurons.

SUPPORTING MATERIAL

Parameters of the active currents in the membrane model and references are available at http://www.biophysj.org/biophysj/supplemental/S0006-3495(09)01508-2.

This work was supported by National Institutes of Health grant NS51382.

REFERENCES

1. Sah, P. 1996. Ca^{2+}-activated K^+ currents in neurones: types, physiological roles and modulation. *Trends Neurosci.* 19:150–154.
2. Kudela, P., P. J. Franaszczuk, and G. K. Bergey. 2003. Reduction of intracellular calcium removal rate can explain changes in seizure dynamics: studies in neuronal network models. *Epilepsy Res.* 57:95–109.
3. Kudela, P., P. J. Franaszczuk, and G. K. Bergey. 2003. Changing excitation and inhibition in simulated neural networks: effects on induced bursting behavior. *Biol. Cybern.* 88:276–285.
4. Abel, H. J., J. C. Lee, J. C. Callaway, and R. C. Foehring. 2004. Relationships between intracellular calcium and afterhyperpolarizations in neocortical pyramidal neurons. *J. Neurophysiol.* 91:324–335.
5. Blaustein, M. P. 1977. Effects of internal and external cations and of ATP on sodium-calcium and calcium-calcium exchange in squid axons. *Biophys. J.* 20:79–111.
6. Koch, C., and I. Segev. 1998. Methods in Neuronal Modeling: From Ions to Networks. MIT Press, Cambridge, MA., 219–220.
7. Gabbiani, F., J. Midtgaard, and T. Knopfel. 1994. Synaptic integration in a model of cerebellar granule cells. *J. Neurophysiol.* 72:999–1009.
8. Blaustein, M. P., and W. J. Lederer. 1999. Sodium calcium exchange: its physiological implications. *Physiol. Rev.* 79:763–854.
9. Gamble, E., and C. Koch. 1987. The dynamics of free calcium in dendritic spines in response to repetitive synaptic input. *Science.* 236:1311–1315.
10. Gorman, A. L., and M. V. Thomas. 1980. Intracellular calcium accumulation during depolarization in a molluscan neurone. *J. Physiol.* 308: 259–285.
11. Smith, S. J., A. B. MacDermott, and F. F. Weight. 1983. Detection of intracellular Ca^{2+} transients in sympathetic neurones using arsenazo III. *Nature.* 304:350–352.